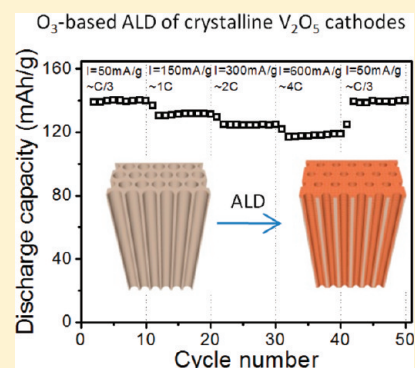


Ozone-Based Atomic Layer Deposition of Crystalline V_2O_5 Films for High Performance Electrochemical Energy StorageXinyi Chen,^{†,‡} Ekaterina Pomerantseva,^{‡,§} Parag Banerjee,^{†,‡} Keith Gregorczyk,^{†,‡} Reza Ghodssi,^{†,‡,§} and Gary Rubloff^{*,†,‡}[†]Department of Materials Science and Engineering, University of Maryland, College Park, Maryland 20742, United States[‡]Institute for Systems Research, University of Maryland, College Park, Maryland 20742, United States[§]MEMS Sensors and Actuators Laboratory, Department of Electrical and Computer Engineering, University of Maryland, College Park, Maryland 20742, United States

ABSTRACT: A new atomic layer deposition (ALD) process for V_2O_5 using ozone (O_3) as oxidant has been developed that resulted in crystalline V_2O_5 thin films which are single-phase and orthorhombic on various substrates (silicon, Au-coated stainless steel, and anodic aluminum oxide (AAO)) without any thermal post-treatment. Within a fairly narrow temperature window (170–185 °C), this low temperature process yields a growth rate of ~ 0.27 Å/cycle on Si. It presents good uniformity on planar substrates. Excellent conformality enables deposition into high aspect ratio (AR) nanopores (AR > 100), as needed for fabrication of three-dimensional (3D) nanostructures for next generation electrochemical energy storage devices. V_2O_5 films obtained using O_3 -based ALD showed superior electrochemical performance in lithium cells, with initial specific discharge capacity of 142 mAh/g in the potential range of 2.6–4.0 V, as well as excellent rate capability and cycling stability. These benefits are attributed primarily to the crystallinity of the material and to fast transport through the thin active storage layers used.

KEYWORDS: atomic layer deposition, vanadium oxide, ozone, electrochemical energy storage



INTRODUCTION

Electrical energy storage is a key challenge for effective use of conventional and renewable energy sources. Applications include electric vehicles, residential energy systems based on renewables, management of distributed and grid level large scale power systems, and portable electronic devices.^{1,2} Electrochemical devices for reversible charge storage, both Li ion batteries and supercapacitors, are needed with high power and high energy density. Three-dimensional (3D) nanostructures offer large surface area, enabling active storage material in the nanostructures to be spatially close to electrolyte, reducing diffusion time for Li transport to fully utilize the active material and thus achieving higher power. However, high density nanostructure arrays, aimed at maintaining high gravimetric and volumetric energy density, require materials synthesis methods capable of conformally coating nanostructures in high aspect ratio (AR) 3D geometries.^{3–5}

Conformal thin film coating methods are required to achieve mechanically stable, binder-free, and high surface area electrodes.^{6,7} Atomic layer deposition (ALD) is a unique thin-film deposition technique which exploits self-limited reactions, leading to monolayer thickness control and unprecedented uniformity and conformality in even the most stringent high AR nanostructures. It is therefore a very promising technique for fabrication of nanoscale heterostructured 3D energy storage devices as we have shown in previous work.^{7,8}

Cathode materials typically limit the energy density of electrochemical storage devices since they have much lower specific capacities compared with anode materials.² Among well-known cathode materials, V_2O_5 offers relatively high specific capacity (147 mAh/g at 2.6–4.0 V; 294 mAh/g at 2.0–4.0 V), fast lithiation, and better safety, which has led to substantial research on its growth and characterization.^{6,9–14} Recently, Cui et al. reported fast, completely reversible Li insertion in V_2O_5 nanoribbons.¹¹ Yu et al. reported mesoporous V_2O_5 nanofibers with significantly enhanced Li-ion storage properties.¹² High performance has also been reported by making V_2O_5 based nanocomposites, including V_2O_5/SnO_2 nanowires,⁶ V_2O_5 -based double-shelled nanocapsules,¹³ and V_2O_5 /carbon nanotubes (CNT) arrays.¹⁴

ALD processes for V_2O_5 are thus attractive for energy storage nanostructures. Significant research has been done using vanadyl triisopropoxide ($VO(OC_3H_7)_3$, VTOP) as the vanadium precursor and water as the oxidant, an ALD process which yielded amorphous films associated with V_2O_5 gel formation from water exposure in the process and subsequent ambient exposure.¹⁵ In order to remove the water and crystallize the film, post annealing above 400 °C was required,

Received: September 27, 2011

Revised: March 2, 2012

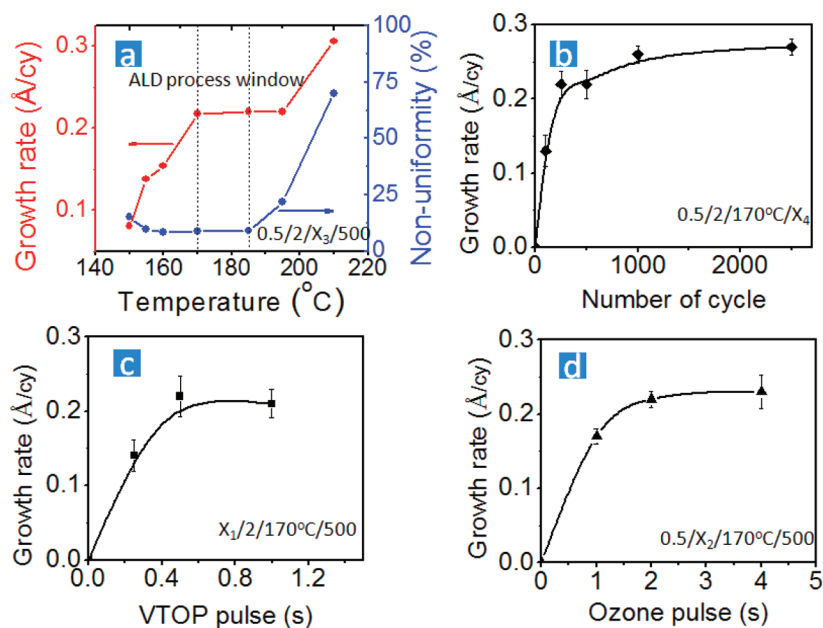


Figure 1. O_3 -based ALD V_2O_5 process (the recipe VTOP pulse/ O_3 pulse/temperature/cycle number is abbreviated as $X_1/X_2/X_3/X_4$): (a) growth rate and nonuniformity across 4" Si wafer as a function of temperature (dotted lines indicate ALD process window); (b) growth rate as a function of cycle number; (c) and (d) saturation behaviors of VTOP and ozone, respectively. Error bars in (b), (c), and (d) indicate standard deviations of thickness across 4" wafer.

posing limitations for the choice of the substrates for electrodes. Recently, Detavernier et al. extended the choices of oxidants to include plasma oxygen in a remote plasma-enhanced ALD process, achieving crystalline V_2O_5 films.¹⁶ However, detailed process development and film properties were not reported.

In this paper, we report a new ozone (O_3)-based ALD process for water-free, well-crystallized V_2O_5 thin film deposition at low temperatures, using VTOP and O_3 precursors with the O_3 delivered directly from an ozone generation system. We report ALD process development and characterization, with analysis of nucleation and film growth mechanism. Seeking energy storage designs which exploit 3D nanoarchitectures, we also report the growth of O_3 -based ALD V_2O_5 over high AR nanopores. Finally, we present electrochemical performance of electrodes made from the as-deposited V_2O_5 films. The results show high specific capacity, excellent rate capability, and cycling stability.

EXPERIMENTAL DETAILS

The ALD V_2O_5 process was developed in BENEQ TFS 500 reactor with a 2 mbar base pressure. $VO(OC_3H_7)_3$ was used as the vanadium precursor, which was kept at 45 °C with a vapor pressure of 0.29 Torr. VTOP pulse is controlled with regular ALD valves, which first introduce N_2 to the precursor supply vessel through an upstream ALD valve, allow the vapor pressure of the VTOP to be established in the N_2 headspace, and then deliver the headspace gas through a downstream ALD valve. Ozone as the oxidizing agent was studied in the ALD V_2O_5 process. A MKS O3MEGA ozone delivery subsystem was employed to supply a stable 18 wt % of O_3 from pure O_2 source. Si wafers were cleaned by a 1 min dip in 1% HF solution, DI water rinsed, and nitrogen blow-dried. The film thickness was measured by a SOPRA GESS Spectroscopic Ellipsometer. The nonuniformity is indicated by the error bars, which were standard deviations from 9 point measurements on Si wafers along the flow direction. Unless otherwise stated, all films for the process development were grown with 500 cycles, each being 0.5 s VTOP pulse, 1 s N_2 purge, 2 s O_3 pulse, and 1 s N_2 purge. Other planar substrates, such as Au-coated stainless steel, and 3D substrates Whatman AAO template (200–300

nm in diameter; 60 μ m thick) were used to characterize the films. These films were grown for 1000 cycles or more.

Morphology for the ALD films was investigated by a Veeco Multimode Atomic Force Microscopy (AFM) with nanoscope III controller, a Hitachi SU-70 High Resolution-Scanning Electron Microscope (SEM) with Energy-Dispersive X-ray spectroscopy (EDX). X-ray diffraction (XRD) was done on a Bruker D8 Advance system with LynxEye PSD detector and Ni β -filter using $CuK\alpha$ radiation (step size 0.02° in the range of 14° < 2 θ < 55°). Raman was performed in a Horiba Jobin-Yvon LabRAM HR-VIS MicroRaman system with an internal 632.8 nm laser source. Thermogravimetric analysis (TGA) was carried out in a TGA Q500 from TA Instruments. The weight loss from the substrate has been subtracted to present the results from V_2O_5 films. The X-ray Photoelectron Spectroscopy (XPS) surface chemistry analysis was done in a custom integrated ultrahigh vacuum system equipped with SPECS surface analysis units and a Veeco ion gun with a 3 cm ion source. The V_2O_5 film was analyzed before and after 2 s ion milling with a beam current of 24 mA to get rid of surface contamination.

The electrochemical properties of the V_2O_5 films prepared by O_3 -based ALD were studied in standard coin cells.⁷ 30 nm V_2O_5 films (around 60 μ g) were first deposited on one side of Au-coated stainless steel disks (1/2" diameter) as the cathode. Then the coin cells were assembled in an Ar-filled glovebox with Li metal as a counter electrode and 1 M $LiPF_6$ solution in ethylene carbonate/diethyl carbonate (EC/DEC, 1:1 by volume) as electrolyte. An Arbin BT-2000 multichannel battery test station was used for galvanostatic and rate capability and life cycle experiments.

RESULTS AND DISCUSSION

ALD Process Development. To investigate wafer scale uniformity, one of the defining parameters for the ALD process, V_2O_5 was deposited on 4" polished Si wafers. The growth rate per cycle (GPC) was determined as a function of deposition temperature from 150 to 210 °C, as shown in Figure 1a. A constant GPC is seen between 170 and 195 °C. Nonuniformity is less than 9% at temperatures between 170 and 185 °C but rapidly increases at higher temperature (right axis of Figure 1a). Therefore, the ALD temperature window is defined as 170–

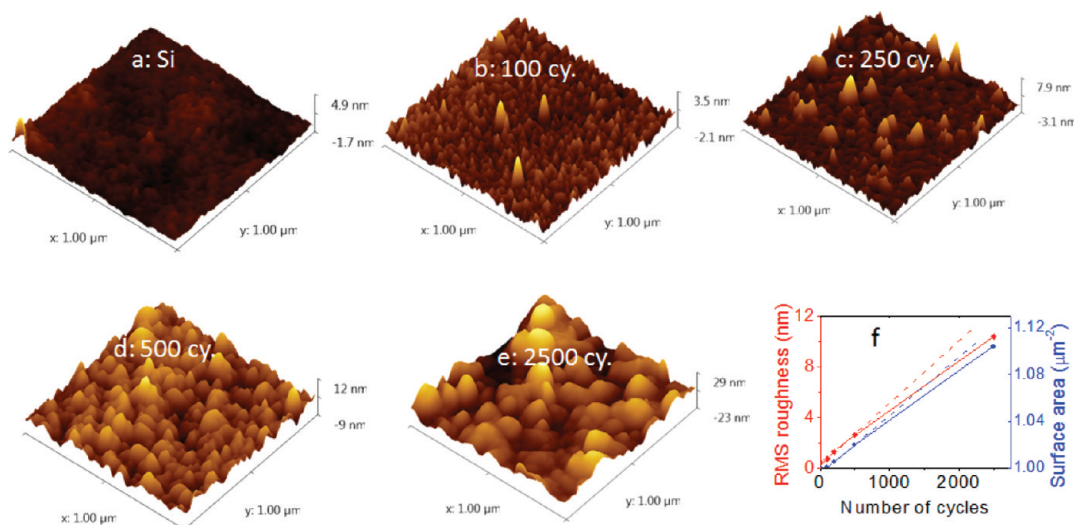


Figure 2. AFM images of (a) Si substrate and ALD V₂O₅ films at (b) 100, (c) 250, (d) 500, and (e) 2500 cycles; (f) rms roughness and surface area (over 1 μm² projected area) as a function of cycle number. Dashed lines are linear fit for 100–500 cycles.

185 °C, where both stable growth rate and uniformity are observed. At temperatures lower than 170 °C, there might be insufficient activation energy for the O₃ to completely react with surface organic ligands, and the saturation for the reaction might take much longer time.¹⁷ Above 185 °C, VTOP starts to decompose resulting in a CVD-like reaction.^{16,18} Combined, these results suggest that the ALD reaction be confined within a narrow temperature window between 170 and 185 °C (Figure 1a). Such low deposition temperatures may enable electrode fabrication by depositing crystalline V₂O₅ on flexible substrates such as polymers and biotemplates.

To understand the deposition kinetics the GPC was monitored as a function of cycle number at a constant temperature of 170 °C (Figure 1b). In principle, the growth rate in an ideal ALD process should be constant regardless of cycle number. However, in our experiments we observed that the film growth rate was only 0.13 Å/cy at 100 cycles and later reached about 0.22 Å/cy at 250 and 500 cycles with a slight increase to 0.27 Å/cy at 2500 cycles. This suggests the dominance of nucleation mechanisms until ~250 cycles for the O₃-based ALD V₂O₅ process, which is confirmed by AFM below.

The saturation behavior of growth rate with precursor dose, also an indicator of ALD behavior, was investigated by monitoring GPC as a function of both VTOP and O₃ pulse times, again at the constant temperature of 170 °C (Figures 1c and 1d). Reaction with VTOP was observed to saturate more quickly (0.5 s pulse) than for ozone (2 s pulse). This may suggest that oxidant is the rate-determining step in the process, which is similar to the H₂O-based ALD process reported by Musschoot et al.¹⁶ and Badot et al.¹⁸

While ALD processes typically reach nonuniformities of just a few % or less, we consider the nonuniformity here (~9% for films with 500 cycles ALD) consistent with the nucleation mechanism. This process involves a significant nucleation barrier, requiring about 250 cycles to initiate stable growth. Nucleation is highly sensitive to surface condition. For the films with 500 cycles ALD, the nucleation period itself comprises a significant contribution to the growth kinetics observed. Varying surface conditions across the sample could well account for variations in nucleation delay, leading to larger

nonuniformities than one might anticipate for an ALD process. It is also found that the nonuniformity generally decreases with the number of cycles; the nonuniformity with more than 1000 cycles was improved to ~4% (see Figure 1b), consistent with our expectation. We also noticed the measured film thicknesses were randomly distributed on the 4" substrate, rather than decreasing along the flow direction, another indication that the slow nucleation accounts for the apparent nonuniformity, rather than unoptimized process for ALD.

To understand the reaction mechanism of the O₃-based V₂O₅ ALD process we considered previous studies on thermal H₂O, O₃, and O₂ plasma-based ALD of Al₂O₃^{19–22} as well as thermal H₂O and O₂ plasma-based ALD of V₂O₅.^{15,16} In the case of Al₂O₃ ALD using trimethylaluminum (TMA) as Al precursor, direct evidence from in situ analysis has suggested combustion-like reaction mechanism for both O₃ and O₂ plasma-based processes. However, the reaction mechanisms vary slightly with oxidability of the oxidants. For example, in the ozone/TMA ALD process, the products involve CH₄, C₂H₄, H₂O, O₂¹⁹ and sometimes CO, CO₂,²⁰ while in the O₂ plasma/TMA case, CH₄, CO, CO₂, H₂O, and O₂ were detected in the products.²¹ In the case of V₂O₅ ALD, Musschoot et al. found through optical emission spectrometry (OES) that CO₂ and H₂O were generated as byproduct in the O₂ plasma-based process. The process yields (001) oriented crystalline V₂O₅ films as a result of a combustion-like mechanism.¹⁶ The mechanism for O₃-based process should also be combustion-like but may differ from O₂ plasma-based process, as indicated by their difference in growth rates (~0.27 Å vs 0.6 Å/cy). The reaction mechanism at 160 °C may also differ from that at 170 °C, as absorption/desorption and oxidability of the oxidants are temperature dependent. However, in situ techniques, such as quadrupole mass spectrometry (QMS), OES, and Fourier transform infrared spectroscopy (FT-IR), must be used for a thorough understanding of the detailed chemical reaction in this process.

Barring steric hindrance effects, ALD growth rates should be close to one monolayer of V₂O₅ per cycle. However, the growth rate of O₃-based ALD of V₂O₅ is ~0.27 Å/cy, which is much lower than one monolayer in (001) plane of crystalline V₂O₅ (*c* = 4.37 Å, one monolayer thickness will be 2.19 Å). It would not

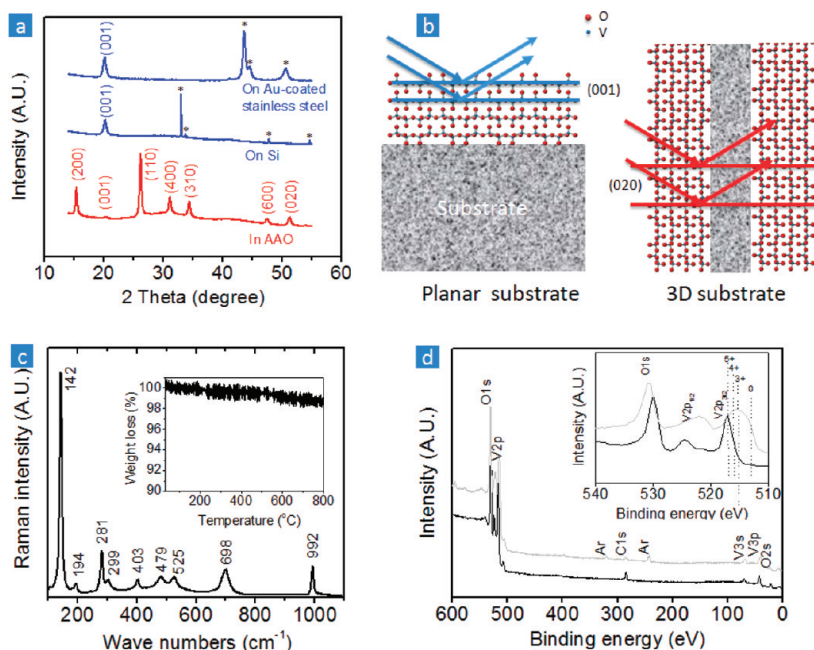


Figure 3. (a) XRD patterns of ALD V_2O_5 films on planar Au-coated stainless steel, Si and in AAO template (peaks marked with stars are from the substrates); (b) illustration of different X-ray diffraction conditions regarding substrate geometries; (c) Raman scattering spectrum of ALD V_2O_5 film on Au-coated stainless steel (inset shows the TGA curve of V_2O_5 films grown in AAO pores); (d) XPS spectra of ALD V_2O_5 before (black) and after (gray) in situ ion milling (inset shows expanded view of $V2p_{3/2}$ peak).

be surprising if reaction involving the large VTOP molecule would be sterically hindered.¹⁷ The growth rate of O_3 -based ALD of V_2O_5 is very similar to the thermal H_2O -based process (~ 0.3 Å/cy) but lower than the O_2 plasma process (~ 0.6 Å/cy).^{15,16} Similar phenomenon has been found in the case of Al_2O_3 ALD, which gives a growth rate of 1.1, 1.1, and 1.7 Å/cy for thermal H_2O , O_3 , and O_2 plasma-based process respectively.²¹ It can be explained that the O_2 plasma pulse generates a higher number of reactive oxide surface groups for metal precursor chemisorption than do the H_2O and O_3 pulses.

Despite the higher growth rate of the O_2 plasma-based process, it is well-known that plasma-enhanced ALD suffers from poor conformality, because of the loss of plasma radicals by surface recombination at the walls of high AR structures.²³ In contrast, O_3 has longer lifetime than O_2 plasma and less surface affinity than H_2O and is therefore considered a better oxidant for conformal ALD coating.^{22,24} What is more, ozone can be readily used in batch processing which is the most effective way around the problem of the low deposition rate in ALD, while with plasma this is much more difficult, if possible at all.

Film Characterization. The morphological evolution of the ALD V_2O_5 films was investigated as a function of cycle number using AFM (Figure 2). Figures 2b-2e clearly show the films are aggregated with nanoparticles, and their size gradually increases with cycle number. After 100 cycles of deposition, an incomplete film with isolated nanoparticles was observed (Figure 2b). At 250 cycles (Figure 2c), nucleation centers coalesce into a complete film and large size particles are denser. This process becomes clearer at 500 cycles (Figure 2d) and 2500 cycles (Figure 2e). From 500 to 2500 cycles it appears that the larger grains dominate growth and surface morphology. Once the V_2O_5 film has achieved complete coverage (around 250 cycles) and nucleation is complete, conformal ALD growth should cause the larger grains to overtake smaller grains and

result in a smoother surface.²⁵ rms roughness and surface area show an initial linear behavior with cycle number and slight sublinear trend at high cycle number (Figure 2f). This is consistent with the improvement in nonuniformity we show in Figure 1b.

The crystallinity of the as-deposited V_2O_5 films was confirmed by XRD, indicating the formation of orthorhombic V_2O_5 phase (JSPDS No. 41-1426), as shown in Figure 3a. V_2O_5 was deposited on three different substrates: Au-coated stainless steel, Si, and nanoporous anodic aluminum oxide (AAO), all showing preferential growth along (001) direction. This is obvious for the films on planar Au-coated stainless steel and Si substrates, since only the (001) peak is observed. Interestingly, in the 3D AAO template, (110) and (200) are the dominant peaks, and the (001) is nearly absent. These results can be understood by recognizing that most of the AAO surface area is vertical, i.e. perpendicular to the plane of the AAO template, so that (001) growth of V_2O_5 on most of the AAO surface area will be in the plane of the template. This is illustrated in Figure 3b, where the (001) face is along the pore wall surface and ineffective in XRD. The faces perpendicular to the (001) face, i.e. (200), are now parallel to the X-ray diffraction plane and observed in the XRD pattern.

The local disorder, bonding, and coordination environments of the V_2O_5 films were studied by Raman spectroscopy. The Raman spectrum shown in Figure 3c is in agreement with the data reported in the literature for the annealed V_2O_5 films, presenting all the peaks of single-phase, well-crystallized V_2O_5 .^{26,27} Typically, the peak at 142 and 992 cm^{-1} corresponds to extension of the V_2O_5 unit cell and $V=O$ stretching vibration modes, respectively. No peaks around 850 cm^{-1} (a typical peak in hydrated V_2O_5)²⁷ were observed, indicating that the films are water-free.

TGA for the V_2O_5 is shown in the inset of Figure 3c. In order to deposit a detectable amount of V_2O_5 for TGA analysis, the

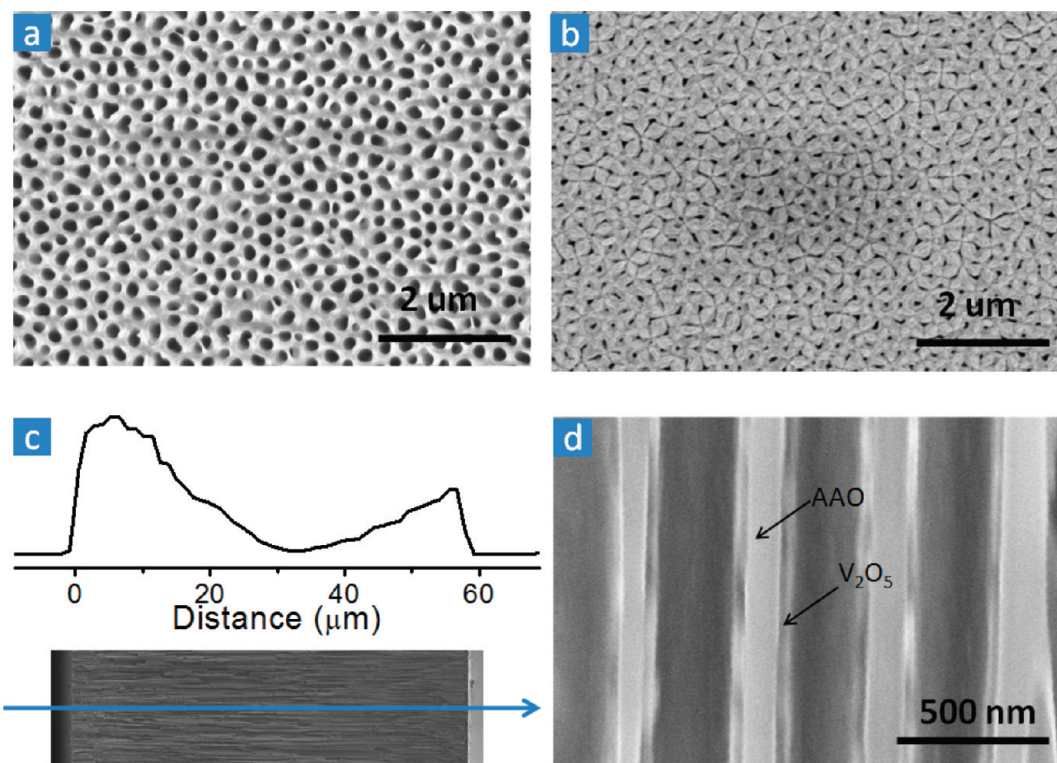


Figure 4. SEM of the AAO template (a) before and (b) after 1000 cycle ozone-based ALD V_2O_5 film deposition; (c) EDX line scan of V signal through the cross-section of V_2O_5 coated AAO template; (d) SEM image of V_2O_5 nanotubes inside AAO pores.

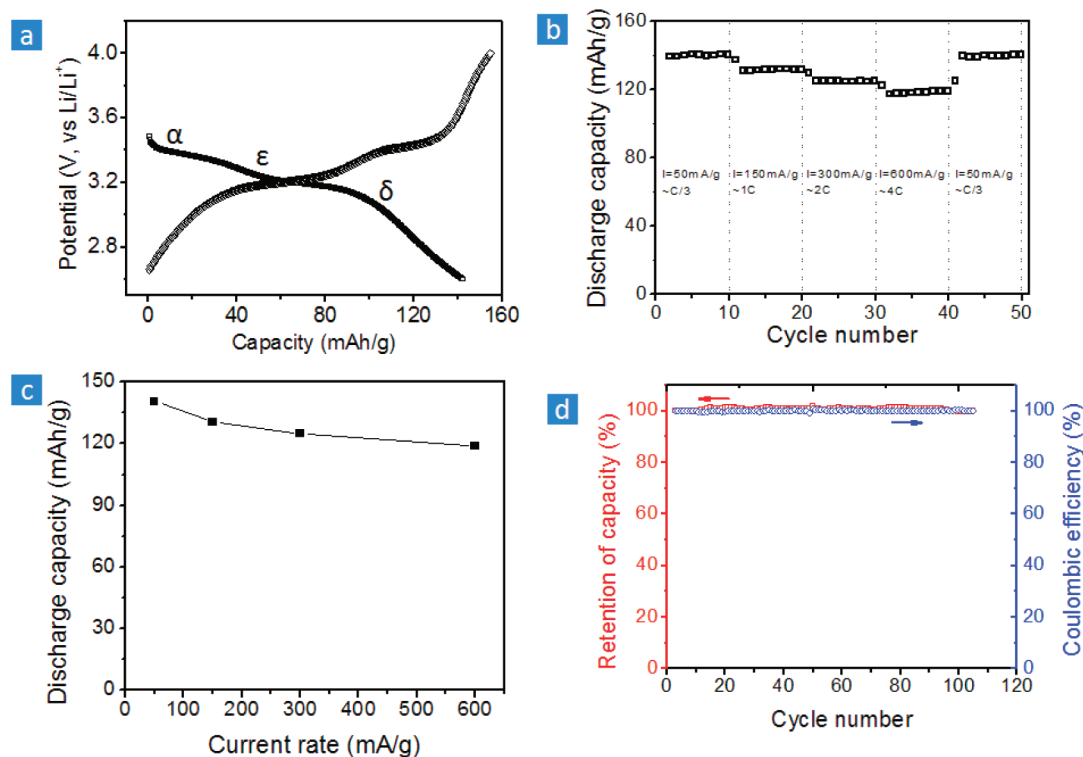


Figure 5. Electrochemical performance of the coin cell with ~ 30 nm thick V_2O_5 film: (a) charge/discharge curve (second cycle, current density of 50 mA/g; phase transition is marked on discharge curve); rate performance at different current densities showing by discharge capacity plotted vs (b) cycle number and (c) current rate; (d) cycling stability and Coulombic efficiency for 105 cycles at ~ 1 C.

highly porous AAO template with high surface area was used as the substrate and 2.5 mg V_2O_5 was successfully deposited inside a 14 mg template after 1000 cycles. A weight loss of only $\sim 1\%$

was detected from room temperature to 800°C , most likely due to absorbed surface contaminants, which further confirms the high purity of the V_2O_5 films.

The XPS spectra (Figure 3d) show that vanadium is in a 5+ valence state, with negligible carbon in the films. In contrast, both carbon and water were detected in the amorphous V_2O_5 films obtained from H_2O -based ALD process,^{15,16,28} We believe the absence of water and carbon residuals in the V_2O_5 films prepared by O_3 -based ALD is critical for the low temperature crystallization behavior.

The reduction of V^{5+} to lower valence state after ion milling is a well-known phenomenon.²⁹ Results for an ion-milled surface compared to the O_3 -based ALD V_2O_5 surface in the inset of Figure 3d are consistent with this.

Conformality. The conformality of the O_3 -based ALD V_2O_5 process in high AR nanostructures was evaluated by deposition into nanopores. The motivation for performing these sets of experiments is to determine the ability of the ALD process for potential electrode applications in complex, high AR nanostructures for batteries and supercapacitors. In these experiments, we chose commercial AAO templates as an extreme case with AR over 100:1 (200–300 nm in diameter, 60 μm thick, both side exposed to precursors). SEM images in Figures 4a and b compare the surface morphology of the AAO template before and after 1000 cycle ALD V_2O_5 coating. Clearly, the pores have been uniformly filled with V_2O_5 on the surface and the pore diameter shrink to around their half size after ALD coating. It is to be noted that the pores remained open after the ALD coating, which is very important for the application in 3D electrodes that require electrolyte to be accessible to deeper part of the pores.

While ALD on planar substrates is primarily determined by self-limiting chemisorption, deposition in 3D nanopore structure involves an additional diffusion (or mass transport) limiting term.²⁵ This means longer precursor exposure times are required to allow the molecules to diffuse into pores and longer carrier gas purge times are needed for unreacted precursor molecules to diffuse out. If the optimized parameters for 2D substrates ($VTOP/N_2/O_3/N_2 = 0.5 \text{ s}/1 \text{ s}/2 \text{ s}/1 \text{ s}$) were used, only the top 15 μm thick template could be coated (not shown here). However, by extending pulse and purge times, i.e., $VTOP/N_2/O_3/N_2 = 4 \text{ s}/2.5 \text{ s}/2 \text{ s}/2.5 \text{ s}$, the V_2O_5 ALD process successfully coated 30 μm deep nanopores. Figure 4c shows a cross-sectional EDX line scan of the vanadium signal along an AAO template, showing that the entire pore was coated. The EDX signal intensity shows notable depletion at the center of the template, i.e. at larger distances from the nanopore openings. Nevertheless the thickness of V_2O_5 is quite well-defined and locally uniform, as shown in the SEM image in Figure 4d.

Electrochemical Performance. Electrochemical performance of the ALD V_2O_5 films ($\sim 30 \text{ nm}$ thick) was evaluated for planar structures in coin cell configurations. The second cycle discharge/charge curves of the lithium cell with ALD V_2O_5 are shown in Figure 5a. The potential window of 2.6–4.0 V corresponding to the theoretical capacity of 147 mAh/g (1 Li^+ (de)/intercalation)³⁰ was chosen due to the good cycling stability delivered by V_2O_5 electrodes in this range. In the extended potential window of 1.8–4.0 V V_2O_5 demonstrates poor cycling stability with the rapidly decreasing capacity.⁶ Two distinct voltage plateaus are observed on both discharge and charge curves, indicating the well-defined phase transformation of α - ϵ - δ .¹⁰ At the second discharge cycle with a current density of 50 mA/g, the capacity of V_2O_5 electrodes is 142 mAh/g, nearly the theoretical capacity of V_2O_5 in the potential window of 2.6–4.0 V.

Figure 5b shows specific discharge capacities obtained for the cells upon cycling at different current rates of 50 ($\sim C/3$), 150 ($\sim 1C$), 300 ($\sim 2C$), and 600 ($\sim 4C$) mA/g. Changes in current density resulted in stepwise capacity drops which are stable at each constant current rate. When the current rate is increased from 50 to 600 mA/g, the specific discharge capacity decreases modestly from 142 to 118 mAh/g, demonstrating good rate performance of the active electrode material. The discharge capacity is also plotted as a function as current rate in Figure 5c. This result is comparable with the V_2O_5 coated SnO_2 nanowire high-power electrodes with $\sim 130 \text{ mAh/g}$ capacity at current rate 500 mA/g.⁶ The specific capacity is recovered from 118 to 142 mAh/g when the current rate decreased from 600 mA/g to the initial value of 50 mA/g and remained 142 mAh/g after total of 50 cycles indicating excellent cycling stability. We also performed longer cycle life tests at 1C rate with 2.6–4.0 V and found there is no decay of the capacity after 105 cycles (Figure 5d). The Coulombic efficiency is 100%, indicating full lithium intercalation/deintercalation.

The power density based on the measured mass of the V_2O_5 film is as high as $\sim 1830 \text{ W/kg}$ with 362 Wh/kg energy density delivered in the 4C test. This value is similar to the power density in a supercapacitor, while our energy density is around 2 orders of magnitude higher. Although the V_2O_5 mass loading on the 1/2" diameter stainless steel disk is only 60 μg , and the stored energy is 0.022 Wh, we found 42 folders enhancement in mass loading in high surface area AAO template (2500 μg V_2O_5 deposited on the same footprint area) due to the ALD conformal coating. Current effort is being made to engineer the AAO-templated 3D electrodes with expected similar enhancement of energy capacity.

We attribute the good electrochemical performance to the high crystallinity of the O_3 -based ALD V_2O_5 material and efficient electron and ion transport through the thin layer of V_2O_5 . The slow ALD growth rate of the process may also have led to stress-free films with excellent mechanical properties. Overall, this work opens new opportunities to develop high performance energy storage devices by exploiting various 3D nanostructures. For example, in a recent publication, we demonstrated that a biotemplated nanostructure coated with O_3 -based ALD V_2O_5 showed 8 times enhancement in areal capacity.³¹ ALD holds great promise for benefit to energy storage technology, though significant technical and manufacturing challenges, especially cost and complexity, remain. Much work is ongoing to develop more viable ALD manufacturing solutions, e.g. roll-to-roll and atmospheric pressure designs.³²

CONCLUSIONS

We have successfully developed and optimized a new ALD V_2O_5 process using O_3 as the oxidant, with an ALD process window between 170 and 185 $^\circ C$ and a steady-state GPC of $\sim 0.27 \text{ \AA/cy}$. Nucleation-controlled growth kinetics are found on Si substrates up to ~ 250 cycles. Surprisingly, and important for electrochemical storage performance, XRD and Raman show the as-deposited films to be crystalline and strongly oriented. TGA and XPS show no carbon or water residuals in the films, which is considered a major reason for the low temperature crystallization behavior. The combustion-like ALD reaction mechanism is proposed, similar to the previous report on a O_2 plasma ALD process. To anticipate applications in 3D nanostructure geometries, conformal coatings were demonstrated in 3D nanopore structures. The electrochemical performance of as-deposited V_2O_5 films on planar electrodes

shows high specific capacity and excellent rate performance and cycling stability. These desirable metrics are attributed primarily to the crystallinity of the material and the use of thin layers for charge storage to achieve fast charge transport.

AUTHOR INFORMATION

Corresponding Author

*Phone: 301-405-3011. Fax: 301-314-2029. E-mail: rubloff@umd.edu. Corresponding author address: 1128 Kim Building, University of Maryland, College Park, MD 20742 USA.

Notes

The authors declare no competing financial interest.

ACKNOWLEDGMENTS

This work has been supported by Nanostructures for Electrical Energy Storage (NEES), an Energy Frontier Research Center funded by the U.S. Department of Energy, Office of Science, Office of Basic Energy Sciences under Award Number DESC0001160. P.B. is partially supported by the John and Maureen Hendricks Foundation. K.G. is partially supported by the L-3 Communications fellowship. The authors wish to acknowledge support of the Maryland NanoCenter and beneficial interactions with Dr. Peter Zavalij (Head of the X-ray Crystallography Center), Dr. Li-Chung Lai at the Nano Center's NispLab, Mr. Wentao Song, Ms. Rennisha Wickham, and Prof. Sang Bok Lee in the Department of Chemistry and Biochemistry.

REFERENCES

- (1) Scrosati, B.; Garche, J. *J. Power Sources* **2010**, *195*, 2419–2430.
- (2) Tarascon, J.; Armand, M. *Nature* **2001**, *414*, 359–367.
- (3) Oudenhoven, J.; Baggetto, L.; Notten, P. *Adv. Energy Mater.* **2011**, *1*, 10–33.
- (4) Golodnitsky, D.; Nathan, M.; Yufit, V.; Strauss, E.; Freedman, K.; Burstein, L.; Gladkikh, A.; Peled, E. *Solid State Ionics* **2006**, *177*, 2811–2819.
- (5) Roberts, M.; Johns, P.; Owen, J.; Brandell, D.; Edstrom, K.; ElEnany, G.; Guery, C.; Golodnitsky, D.; Lacey, M.; Lecoeur, C.; Mazor, H.; Peled, E.; Perre, E.; Shaijumon, M.; Simonc, P.; Taberna, P. *J. Mater. Chem.* **2011**, *21*, 9876.
- (6) Yan, J.; Sumboja, A.; Khoo, E.; Lee, P. *Adv. Mater.* **2011**, *23*, 746–750.
- (7) Gerasopoulos, K.; Chen, X.; Culver, J.; Wang, C.; Ghodssi, R. *Chem. Commun.* **2010**, *46*, 7349.
- (8) Banerjee, P.; Perez, I.; Henn-Lecordier, L.; Lee, S.; Rubloff, G. *Nat. Nanotechnol.* **2009**, *4*, 292–296.
- (9) Braithwaite, J.; Catlow, C.; Gale, J.; Harding, J. *Chem. Mater.* **1999**, *11*, 1990–1998.
- (10) Whittingham, M.; Song, Y.; Lutta, S.; Zavalij, P.; Chernova, N. *J. Mater. Chem.* **2005**, *15*, 3362.
- (11) Chan, C.; Peng, H.; Twisten, R.; Jarausch, K.; Zhang, X.; Cui, Y. *Nano Lett.* **2007**, *7*, 490–495.
- (12) Yu, D.; Chen, C.; Xie, S.; Liu, Y.; Park, K.; Zhou, X.; Zhang, Q.; Li, J.; Cao, G. *Energy Environ. Sci.* **2011**, *4*, 858.
- (13) Liu, J.; Xia, H.; Xue, D.; Lu, L. *J. Am. Chem. Soc.* **2009**, *131*, 12086–12087.
- (14) Seng, K.; Liu, J.; Guo, Z.; Chen, Z.; Jia, D.; Liu, H. *Electrochem. Commun.* **2011**, *13*, 383–386.
- (15) Banerjee, P.; Chen, X.; Gregorczyk, K.; Henn-Lecordier, L.; Rubloff, G. *J. Mater. Chem.* **2011**, *21*, 15391–15397.
- (16) Musschoot, J.; Deduytsche, D.; Poelman, H.; Haemers, J.; Meirhaeghe, R.; Berghe, S.; Detavernier, C. *J. Electrochem. Soc.* **2009**, *156*, 122.
- (17) George, S. *Chem. Rev.* **2010**, *110*, 111–131.
- (18) Badot, J.; Riber, S.; Yousfi, E.; Vivier, V.; Pereira-Ramos, J.; Baffier, N.; Lincot, D. *Electrochem. Solid State Lett.* **2000**, *3*, 485–488.
- (19) Elliott, S.; Scarel, G.; Wiemer, C.; Fanciulli, M.; Pavia, G. *Chem. Mater.* **2006**, *18*, 3764–3773.
- (20) Goldstein, D.; McCormick, J.; George, S. *J. Phys. Chem. C* **2008**, *112*, 19530–19539.
- (21) Heil, S.; Kudlacek, P.; Langereis, E.; Engeln, R.; Sanden, M.; Kessels, W. *Appl. Phys. Lett.* **2006**, *89* (13), 131505.
- (22) Rose, M.; Niinisto, J.; Endler, I.; Bartha, J.; Kucher, P.; Ritala, M. *ACS Appl. Mater. Interfaces* **2010**, *2* (2), 347–350.
- (23) Dendooven, J.; Deduytsche, D.; Musschoot, J.; Vanmeirhaeghe, R.; Detavernier, C. *J. Electrochem. Soc.* **2010**, *157* (4), G111.
- (24) Henn-Lecordier, L.; Anderle, M.; Robertson, E.; Rubloff, G. *J. Vac. Sci. Technol. A* **2011**, *29* (5), 051509.
- (25) Cleveland, E.; Banerjee, P.; Perez, I.; Lee, S.; Rubloff, G. *ACS Nano* **2010**, *4*, 4637–4644.
- (26) Baddour-Hadjean, R.; Golabkan, V.; Pereira-Ramos, J.; Mantoux, A.; Lincot, D. *J. Raman Spectrosc.* **2002**, *33*, 631–638.
- (27) Sanchez, C.; Livage, J.; Lucazeau, G. *J. Raman Spectrosc.* **1982**, *12*, 1.
- (28) Van, K.; Groult, H.; Mantou, A.; Perrigaud, L.; Lantelme, F.; Lindström, R.; Badour-Hadjean, R.; Zanna, S.; Lincot, D. *J. Power Sources* **2006**, *160*, 592–601.
- (29) Silversmit, G.; Depla, D.; Poelman, H.; Marin, G.; Gryse, R. *Surf. Sci.* **2006**, *600*, 3512–3517.
- (30) Whittingham, M. *Chem. Rev.* **2004**, *104*, 4271–4301.
- (31) Pomerantseva, E.; Gerasopoulos, K.; Chen, X.; Rubloff, G.; Ghodssi, R. *J. Power Sources* **2012**, *206*, 282–287.
- (32) Parsons, G.; George, S.; Knez, M. *MRS Bull.* **2011**, *36*, 865–871.